Food Bioscience 47 (2022) 101623

Contents lists available at ScienceDirect

Food Bioscience

journal homepage: www.elsevier.com/locate/fbio

Isolation of chemical compositions as dietary antioxidant supplements and neuroprotectants from Chaga mushroom (*Inonotus obliquus*)

Ye Chang [a,b,c,d,1], Ming Bai [a,b,c,d,1], Xiao-Bian Xue [a,b,c,d], Chun-Xin Zou [a,b,c,d], Xiao-Xiao Huang [a,b,c,d], Shao-Jiang Song [a,b,c,d,*]

[a] Key Laboratory of Computational Chemistry-Based Natural Antitumor Drug Research & Development, Liaoning Province, China
[b] Engineering Research Center of Natural Medicine Active Molecule Research & Development, Liaoning Province, China
[c] Key Laboratory of Natural Bioactive Compounds Discovery & Modification, Shenyang, China
[d] School of Traditional Chinese Materia Medica, Shenyang Pharmaceutical University, Shenyang, Liaoning, 110016, China

ARTICLE INFO

Keywords:
Inonotus obliquus
Chaga mushroom
Functional food
Neuroprotective activity
Antioxidant activity

ABSTRACT

Excessive free radicals can cause oxidative stress (OS), which lead to neurodegenerative diseases (ND) are harmful to the human body. Therefore, it is necessary to explore dietary antioxidants and neuroprotectants from nutrient foods. Chaga mushroom (*Inonotus obliquus*) has been used as an important functional food in many countries for centuries. This present study was carried out to discover active compounds from *I. obliquus* and investigate the *in vitro* antioxidant activity and neuroprotective activity. Sixteen natural products including two new isocoumarins (**1**–**2**), a new 8-*O*-4′-neolignan (**3**), a new cyclic diarylheptanoid (**4**), and twelve known compounds (**5**–**16**) were separated from *I. obliquus*. Their structures were elucidated by extensive spectroscopic analyses of high resolution electrospray mass spectrometry (HRESIMS), ultra violet (UV), and nuclear magnetic resonance (NMR). Among them, compounds **1** and **2** revealed remarkable antioxidant activities through the comprehensive analysis of DPPH, ABTS, and ferric reducing antioxidant power (FRAP) methods. Meanwhile, compound **1** demonstrated significant neuroprotective activity by increasing SH-SY5Y cells viability and preventing mitochondrial damage. Apart from that, electronic analyses were performed using the highest occupied molecular orbital (HOMO), and the lowest unoccupied molecular orbital (LUMO) to analyze compound **1**. These results indicated that compound **1** had a significant implication for the search of natural raw material to prevent OS and nerve damage in the field of functional foods, and the isocoumarin fragment as well as an oxygenated *cis* double-bond might be the active sites to play prominent parts in antioxidant and neuroprotective activities of compound **1**.

1. Introduction

Excess free radicals can cause oxidative stress (OS) and lead to several diseases such as neurodegenerative diseases (ND), stroke, autoimmune disorders, and cancers (Di Meo & Venditti, 2020). Parkinson's disease (PD), Alzheimer's disease (AD), and Huntington's disease (HD) are common ND that makes neuronal cells become dysfunctional and cause damage to the central nervous system, peripheral nerves, and muscles (Radi et al., 2014). Common free radicals, such as reactive oxygen species (ROS), may trigger OS when their levels increase (Liu et al., 2021). The nerve cell damage induced by this phenomenon is closely related to ND and is also an important cause of their pathogenesis (Alkadi, 2020; Bhat et al., 2015; Li et al., 2021). Antioxidants are divided into endogenous antioxidants produced in the human body and exogenous antioxidants obtained from foods or nutrients (Alkadi, 2020; Neha et al., 2019). According to research, exogenous antioxidants such as vitamin C and vitamin E obtained through the diet are also a class of dietary antioxidants that contribute greatly to helping patients with ND (Albarracin et al., 2012; Zia & Alibas, 2021). Therefore, it is of great significance to screen for dietary antioxidant supplements and neuroprotectants from natural foods that are effective in weakening OS to develop benefits for human health.

Inonotus obliquus, as a well-known Chaga mushroom, grows on the barks and kraurotic trunks of birch trees and is widely distributed in Russia, Northern China, Japan, as well as in United States, Korea, and

* Corresponding author. Key Laboratory of Computational Chemistry-Based Natural Antitumor Drug Research & Development, Liaoning Province, China.
E-mail address: songsj99@163.com (S.-J. Song).
[1] These authors contributed equally to this study.

https://doi.org/10.1016/j.fbio.2022.101623
Received 27 October 2021; Received in revised form 7 February 2022; Accepted 16 February 2022
Available online 19 February 2022

Abbreviations

ABTS	2,2'-azino-bis(3-ethylbenzothiazoline-6-sulfonic acid) diammonium salt
AD	Alzheimer's disease
ANOVA	Analysis of variance
$CDCl_3$	Chloroform-*d*
CH_2Cl_2	Dichloromethane
COSY	Two-dimensional shift correlated spectroscopy
DFT	Density functional theory
DMEM	Dulbecco's modified Eagle's medium
DMSO	Dimethyl sulfoxide
DMSO-d_6	Dimethyl sulfoxide-d_6
DPPH	2,2-diphenyl-1-(2,4,6-trinitrophenol)hydroxyl
ECD	Electronic circular dichroism
EtOAc	Ethyl acetate
EtOH	Ethyl alcohol
FRAP	Ferric reducing antioxidant power
H_2O_2	Hydrogen peroxide
H_2O	Water
HD	Huntington's disease
HMBC	Heteronuclear multiple bond correlation
Hoechst 33258	2'-(4-hydroxyphenyl)-5-(4-methyl-1-piperazinyl)-2,5′-bi-1H-benzi midazole
HOMO	Highest occupied molecular orbital
HPLC	High-performance liquid chromatography
HRESIMS	High resolution electrospray mass spectrometry
HSQC	Heteronuclear single quantum correlation
JC-1	5,5′,6,6′-tetrachloro-1,1,3,3′-tetraethylbenzimidizolyl carbocyanine iodide
LUMO	Lowest unoccupied molecular orbital
MeCN	Acetonitrile
MeOH	Methanol
MMP	Mitochondrial membrane potential
MTT	3-(4,5-dimethylthiazol-2-yl)-2,5-diphenyl-2Htetrazolium bromide
n-BuOH	Normal butanol
ND	Neurodegenerative diseases
NMR	Nuclear magnetic resonance
NOESY	Nuclear overhauser effect spectroscopy
ODS	Octadecylsilyl silica
OS	Oxidative stress
PBS	Phosphate-buffered saline
PCM	Polarizable continuum model
PD	Parkinson's disease
ROS	Reactive oxygen species
SD	Standard deviation
TDDFT	Time-dependent density functional theory
TMS	Tetramethylsilane
TPTZ	2,4,6-tripyridyl-s-triazine
UV	Ultra violet
VLC	Vacuum liquid chromatography

Siberia (Ma et al., 2013; Zheng et al., 2010). In the field of functional foods, *I. obliquus* had been developed into a range of health products, such as Chaga mushroom capsules, mushroom concentrate powders, and functional drinks (Chen et al., 2021). On the other hand, it had also been drunk as a tea in Japan and Russia for centuries because of its health benefits (Liang et al., 2009; Yu et al., 2020). *I. obliquus* has great potential to become a natural and edible antioxidant due to its remarkable antioxidant capacity to maintain a balance between the oxidative system and free radicals in the human body (Wang et al., 2018; Xiang et al., 2012; Xu et al., 2011). In conjunction with previous studies, Chaga mushroom is rich in aromatic compounds with polyphenolic hydroxyl groups (Lee et al., 2007), which may have the potential to protect the body from diseases caused by OS.

Therefore, in order to obtain more bioactive compounds from *I. obliquus*, this article conducts chemically investigation, evaluates antioxidant and neuroprotective capacity as well as analyzes active sites. Meanwhile, the purpose of this study is to discover raw material for dietary antioxidant supplements and neuroprotectants with significant biological activities from Chaga mushroom for protecting human body from diseases caused by OS and nerve damage. The results of experiments will reveal the types of compounds and pharmacological activities in *I. obliquus*, and provide a scientific basis for searching dietary antioxidant supplements and neuroprotectants.

2. Materials and methods

2.1. Fungal material

The sclerotia of *I. obliquus* was collected in Siberia, Russia in 2016. The species identification was confirmed by Prof. Yi-Xuan Zhang (School of Life Sciences and Biopharmaceutical Science). A voucher specimen (No.20160626) was deposited at the herbarium of Shenyang Pharmaceutical University, Shenyang, Liaoning Province, PR China.

2.2. General experimental procedures

Optical rotations were determined using a JASCO DIP-370 digital polarimeter (Jasco, Tokyo, Japan) in methanol (MeOH) at 20 °C. Ultra violet (UV) was measured using the Shimadzu UV-1700 spectrophotometer (Shimadzu, Kyoto, Japan). Electronic circular dichroism (ECD) measurements were carried out on a Bio-Logic MOS 450 spectrophotometer (Bio-Logic Science Instruments, Seyssinet-Pariset, France). Nuclear magnetic resonance (NMR) spectra were measured with a Bruker AVIII-600 spectrometer (600 and 150 MHz for ^1H and ^{13}C, respectively) (Bruker Corp., Bremen, Germany) with dimethyl sulfoxide-d_6 (DMSO-d_6) and chloroform-*d* ($CDCl_3$) as solvents and MHz spectrometers using tetramethylsilane (TMS) as the internal standard. High-resolution electrospray mass spectrometry (HRESIMS) analyses were performed on a Bruker Micro Q-TOF instrument (Bruker Daltonics, Billerica, MA, USA) in positive-ion mode. Semipreparative high-performance liquid chromatography (HPLC) system (YMC gel C_{18} column, 250 mm × 10 mm, 5 μm, Shimadzu) was performed using an instrument equipped with a LC-6AD pump (Shimadzu) and a SPD-20A ultraviolet–visible light absorbance detector (Shimadzu). Column chromatography was performed with silica gel (100∼200 or 200∼300 mesh, Qingdao Marine Chemical Inc., Qingdao, Shandong, China), HP-20 macroporous resin (75∼150 μm, Mitsubishi Chemical Co., Ltd., Tokyo, Japan) and octadecylsilyl silica (ODS) gel (60∼80 μm, Merck, Darmstadt, Germany). All solvents were of analytical grade except for the chromatographic grade MeOH and acetonitrile (MeCN) for HPLC separations. The chemicals used in the experimental process were all purchased from Sigma-Aldrich (Steinheim, Germany).

Besides, DPPH (2,2-diphenyl-1-(2,4,6-trinitrophenol)hydroxyl), ABTS (2,2′-azino-bis(3-ethylbenzothiazoline-6-sulfonic acid) diammonium salt), TPTZ (2,4,6-tripyridyl-s-triazine), and Trolox were all purchased from Sigma-Aldrich in order to test the antioxidant capacities of scavenging reactive oxidants of the isolated compounds.

2.3. Extraction and isolation

The air-dried sclerotia of *I. obliquus* (30 kg) was soaked with 70 L of 70% ethyl alcohol (EtOH), for 2 h at 70 °C for three times, and evaporated under reduced pressure to obtain a crude extract. This extract (1200 g) was suspended in distilled water and partitioned sequentially with 15 L of ethyl acetate (EtOAc) and 42 L of normal butanol (*n*-BuOH), to give EtOAc-soluble (277 g) and *n*-BuOH-soluble extracts (764 g), respectively. The EtOAc-soluble fraction was separated by vacuum liquid chromatography (VLC) on a silica gel column chromatography using a step gradient elution of dichloromethane (CH_2Cl_2)/MeOH (CH_2Cl_2, 24 L; MeOH, 12 L; from 50:1 to 1:2, v:v) to obtain three fractions (Fr.1 to Fr.3). Fr.1 (46 g) was fractionated using column chromatography over ODS and eluted with EtOH/Water (H_2O) (from 10:90 to 100:0, v:v) to afford three fractions (Fr.1.1 to Fr.1.3). Fr.1.1 (15 g) was purified by semi-preparative HPLC with solvent system MeCN/H_2O (15:85, 2.5 mL/min) to yield **6** (13.0 mg), **7** (15.7 mg), **8** (120.0 mg), **10** (4.9 mg), **11** (4.6 mg), **14** (2.6 mg) and **15** (2.6 mg). Fr.1.2 (17 g) was passed over a preparative HPLC, eluted with MeCN/H_2O (20:80, 2.5 mL/min), to give **2** (13.6 mg) and **9** (36 mg). Fr.1.3 (9 g) was purified by chromatography on a semi-preparative HPLC-C_{18} column and eluted with a mixture of MeCN/H_2O (35:65, 2.5 mL/min), affording compounds **1** (8.9 mg) and **5** (4.6 mg). Fr.2 (101 g) was separated by HP-20 macroporous resin with EtOH/H_2O (from 30:70 to 90:10, v:v) to yield three subfractions (Fr.2.1a to Fr.2.1c). Three subfractions were severally loaded on an ODS column eluting with EtOH/H_2O (from 10:90 to 100:0, v:v) and precisely analyzed with HPLC to obtain five pooled subfractions (Fr.2.1.1 to Fr.2.1.5). Fr.2.1.1 (15 g) was further refined by reversed-phase C_{18} column chromatography with MeCN/H_2O (17:83, 2.5 mL/min) to provide compounds **13** (3.1 mg) and **16** (5.2 mg). Compounds **3** (5.3 mg) and **12** (3.1 mg) were obtained from Fr.2.1.3 (9 g) by preparative HPLC on a YMC RP-C_{18} column with a gradient of MeCN/H_2O (41:59, 2.5 mL/min). Fr.2.1.4 (11.0 g) was eluted with an isopycnic gradient of MeCN/H_2O (49:51, 2.5 mL/min) to yield **4** (4.7 mg).

Phellxinye A (**1**): Light yellow powder; [α] +214.0; UV (MeOH) λ_{max} (log ε) 202 (1.05), 257 (0.45) nm; HRESIMS *m/z* 659.0646 $[M + Na]^+$ (calcd for $C_{30}H_{20}O_{16}Na$, 659.0644); ^1H NMR (600 MHz, DMSO-d_6): δ_H 8.35 (1H, s, H-10), 8.28 (1H, s, H-5′), 7.54 (1H, s, H-7), 7.49 (1H, s, H-8′), 7.37 (1H, s, H-4), 6.59 (1H, s, H-9′), 3.90 (3H, s, 14′-OCH_3), 3.62 (3H, s, 13′-OCH_3), 2.86 (2H, t, J = 7.3 Hz, H-11′), 2.73 (2H, t, J = 7.3 Hz, H-12′); ^{13}C NMR (150 MHz, DMSO-d_6): δ_C 171.9 (C-13′), 163.8 (C-10′), 160.6 (C-3′), 160.0 (C-4a), 159.0 (C-14′), 158.6 (C-1′), 158.5 (C-11), 158.4 (C-6), 158.2 (C-1), 153.7 (C-9), 153.7 (C-6′), 148.3 (C-8), 147.0 (C-7′), 146.5 (C-3), 126.6 (C-4′a), 125.6 (C-10a), 114.6 (C-7), 114.4 (C-8′), 112.5 (C-6a), 111.4 (C-8′a), 111.1 (C-10), 110.5 (C-5′), 104.4 (C-10b), 106.3 (C-4), 99.0 (C-9′), 98.5 (C-4′), 53.3 (14′-OCH_3), 51.7 (13′-OCH_3), 30.0 (C-12′), 28.2 (C-11′).

Inonotphenol A (**2**): Brown powder; [α] -7.0; UV (MeOH) λ_{max} (log ε) 245 (1.60) nm; HRESIMS *m/z* 251.0561 $[M + H]^+$ (calcd for $C_{12}H_{11}O_6$, 251.0550); ^1H NMR (600 MHz, DMSO-d_6): δ_H 7.43 (1H, s, H-8), 7.04 (1H, s, H-5), 3.88 (3H, s, 10-OCH_3), 2.31 (3H, s, H-9); ^{13}C NMR (150 MHz, DMSO-d_6): δ_C 166.1 (C-10), 159.7 (C-1), 155.0 (C-3), 153.8 (C-6), 146.9 (C-7), 128.2 (C-4a), 113.3 (C-8), 110.5 (C-8a), 109.2 (C-5), 109.0 (C-4), 52.4 (10-OCH_3), 18.7 (C-9).

***Erythro*-4,7,9,9′-tetrahydroxy-3,5,3′,5′-tetramethoxy-8-*O*-4′-neolignan** (**3**): Yellow oil; [α] -6.0; UV (MeOH) λ_{max} (log ε) 206 (2.65), 277 (0.41) nm; HRESIMS *m/z* 475.1576 $[M + Na]^+$ (calcd for $C_{22}H_{28}O_{10}Na$, 475.1575); ^1H NMR (600 MHz, DMSO-d_6): δ_H 8.31 (1H, s, 4-OH), 7.22 (2H, s, H-2′/6′), 6.60 (2H, s, H-2/6), 4.80 (1H, d, J = 4.9 Hz, H-7), 4.36 (1H, dt, J = 4.9, 3.5 Hz, H-8), 3.83 (6H, s, 3′/5′-OCH_3), 3.77 (2H, t, J = 6.3 Hz, H-9′), 3.72 (6H, s, 3/5-OCH_3), 3.71 (1H, m, H-9a), 3.49 (1H, dd, J = 11.9, 3.5 Hz, H-9b), 3.13 (2H, t, J = 6.3 Hz, H-8′); ^1H NMR (600 MHz, $CDCl_3$): δ_H 7.29 (2H, s, H-2′/6′), 6.58 (2H, s, H-2/6), 4.99 (1H, d, J = 3.3 Hz, H-7), 4.23 (1H, dt, J = 6.6, 3.5 Hz, H-8), 4.05 (2H, t, J = 5.2 Hz, H-9′), 3.96 (6H, s, 3′/5′-OCH_3), 3.92 (1H, overlap, H-9a), 3.88 (6H, s, 3/5-OCH_3), 3.53 (1H, d, J = 12.0 Hz, H-9b), 3.23 (2H, t, J = 5.3 Hz, H-8′); ^{13}C NMR (150 MHz, DMSO-d_6): δ_C 197.9 (C-7′), 152.4 (C-3′/5′), 147.4 (C-3/5), 140.6 (C-4′), 134.4 (C-4), 132.4 (C-1), 131.6 (C-1′), 105.7 (C-2′/6′), 104.3 (C-2/6), 86.5 (C-8), 72.4 (C-7), 60.2 (C-9), 57.1 (C-9′), 56.1 (C-3′/5′-OCH_3), 55.9 (C-3/5-OCH_3), 41.2 (C-8′)

(9*S*)-acerogenin M (**4**): Yellow oil; [α] -36.0; UV (MeOH) λ_{max} (log ε) 209 (3.30), 230 (2.80), 277 (1.70) nm; HRESIMS *m/z* 335.1254 $[M + Na]^+$ (calcd for $C_{19}H_{20}O_4Na$, 335.1254); ^1H NMR (600 MHz, $CDCl_3$): δ_H 7.52 (1H, dd, J = 8.4, 2.1 Hz, H-4), 7.31 (1H, overlap, H-19), 7.31 (1H, overlap, H-15), 7.20 (1H, dd, J = 8.5, 2.5 Hz, H-16), 7.02 (1H, d, J = 8.4 Hz, H-3), 6.96 (1H, dd, J = 8.7, 2.5 Hz, H-18), 6.03 (1H, d, J = 2.1 Hz, H-6), 3.32 (1H, m, H-9), 2.99 (1H, dd, J = 13.0, 1.6 Hz, H-8a), 2.84 (1H, m, H-13a), 2.59 (1H, m, H-13b), 2.07 (1H, dd, J = 13.0, 9.7 Hz, H-8b), 1.76 (1H, m, H-12a), 1.50 (1H, m, H-12b), 1.44 (1H, m, H-10a), 1.24 (1H, m, H-10b), 1.15 (1H, m, H-11a), 0.90 (1H, m, H-11b); ^{13}C NMR (150 MHz, $CDCl_3$): δ_C 199.1 (C-7), 154.3 (C-17), 149.6 (C-2), 148.6 (C-1), 141.4 (C-14), 132.0 (C-15), 131.3 (C-19), 129.5 (C-5), 123.7 (C-18), 123.2 (C-16), 122.8 (C-4), 117.4 (C-6), 116.3 (C-3), 70.1 (C-9), 46.6 (C-8), 37.5 (C-10), 35.0 (C-13), 32.3 (C-12), 21.8 (C-11).

2.4. DPPH scavenging activity

The free radical-scavenging potentials of all isolated compounds were appraised using DPPH (Ghalkhani et al., 2021), a stable free radical, which obtained a center of a nitrogen atom. The DPPH free radicals turned into stabilized DPPH molecules and causing the color to change from deepest purple to pale yellow after scavenging reactive oxidants and a specific absorption at 517 nm was observed by the UV spectrophotometer. Diluted compounds **1**–**16** (100 μL) with various concentrations (200, 100, 50, 25, 10 μg/mL) prepared in absolute EtOH were added to 100 μL of DPPH solution (0.2 mmol/L) and Trolox was considered as a positive reference. The absorbances of the reaction mixture after a 30 min adequate incubation at ambient temperature (25 °C) were measured at room temperature (25 °C) in the dark. The DPPH scavenging activities were calculated according to the following equation:

$$\text{DPPH scavenging activity } (\%) = [1 - (A_s - A_b) / A_0] \times 100\%$$

Where A_s is the absorbance of the tested sample, A_b is the absorbance of the contrast group and A_0 is the absorbance of black control.

2.5. ABTS scavenging activity

The ABTS radical scavenging assay by some certain steps with slight modifications (Otmani et al., 2021). The specific operation was as follows: ABTS solution was suitably diluted with prepared phosphate-buffered saline (PBS) solution so that its absorbance reached about 0.70 at 734 nm. Subsequently, 100 μL of different concentrations of above compounds (200, 100, 50, 25, 10 μg/mL) were blended with 150 μL of ABTS radical cation solution thoroughly and measured as (A_s). The test mixture consisted of 100 μL (200, 100, 50, 25, 10 μg/mL) of samples and 150 μL of PBS solution, and the absorbance was measured and expressed as (A_b). A mixture of 100 μL of absolute EtOH and 150 μL of ABTS solution was used as a blank control and the value of absorbance was presented with A_0. Finally, the reaction was carried out for 6 min at room temperature and protected from light in 96-well plates (Nest Biotech, Co., Ltd., Wuxi, Jiangsu, China), and the absorbance values at 734 nm were perused. The ABTS radical scavenging rate can be calculated by the following formula:

$$\text{ABTS scavenging activity } (\%) = [1 - (A_s - A_b) / A_0] \times 100\%$$

Where As is the absorbance of the tested sample, Ab is the absorbance of the contrast group and A0 is the absorbance of black control.

2.6. FRAP scavenging activity

The total antioxidant capacity was assessed through ferric reducing antioxidant power (FRAP) method (Zuriarrain-Ocio et al., 2021). Illustration of the strength and weakness of antioxidant activity by comparing the capacity of reduction of trivalent ferric tripyridyltriazine (Fe^{3+}-TPTZ) transform into ferrous form (Fe^{2+}-TPTZ). The standard curve (Y = 0.0109X − 0.124) was prepared by taking varies linearly with concentrations of Ferrous sulfate. The absorbance at 593 nm of 150 μL of FRAP working solution and 5 μL of different concentrations (200, 100, 50, 25, 10 μg/mL) of the samples were measured after 30 min of full reaction with 145 μL of FRAP working solution at 37 °C and were recorded as A_x and A_{x0}. The differences between A_x and A_{x0} were calculated and the values were subsequently brought into the standard curve to obtain the corresponding FRAP values.

2.7. Cell culture and MTT assay

For this experiment, the human neuroblastoma cell line SH-SY5Y (ATCC, Manassas, VA, USA) was cultured in DMEM (Dulbecco's modified Eagle's medium) (Thermo Scientific, Logan, UT, USA) supplemented with 10% fetal bovine serum (Thermo Scientific) and 1% penicillin G (Thermo Scientific) was added into the medium in 96-well plates at an initial density of 1.2×10^4 cells/mL. Afterward, the suspended cells were grown at 37 °C with 5% CO_2 and 90% relative humidity condition to incubate for 12 h in the incubator (Thermo Scientific). After overnight incubation, SH-SY5Y cells were treated with the tested compounds at a series of concentrations (12.5, 25 and 50 μmol/L) for 1 h and then treated with hydrogen peroxide (H_2O_2) (300 μmol/L) (Tianjin Hengxing Chemical Reagents Co., Ltd., Tianjin, China) incubated for 4 h. Subsequently, 20 μL of MTT (3-(4,5-dimethylthiazol-2-yl)-2,5-diphenyl-2Htetrazolium bromide) (Sigma, St. Louis, MO, USA) solution (5 mg/mL in PBS) was added into each well and incubated for 4 h in the dark. After adding 150 μL of dimethyl sulfoxide (DMSO) into each well, the optical density of formazan crystals was recorded at 490 nm by a microplate reader (Thermo, Waltham, MA, USA). Trolox and DMSO were used as positive and negative controls, respectively. The experiments were carried out in triplicate and the neuroprotective activities of compounds were determined by MTT assay (Li, Lu, et al., 2020). The cell viability was calculated as follows:

$$\text{Cell viability (\%)} = [(A_{490,\text{sample}} - A_{490,\text{blank}})/(A_{490,\text{control}} - A_{490,\text{blank}})] \times 100\%$$

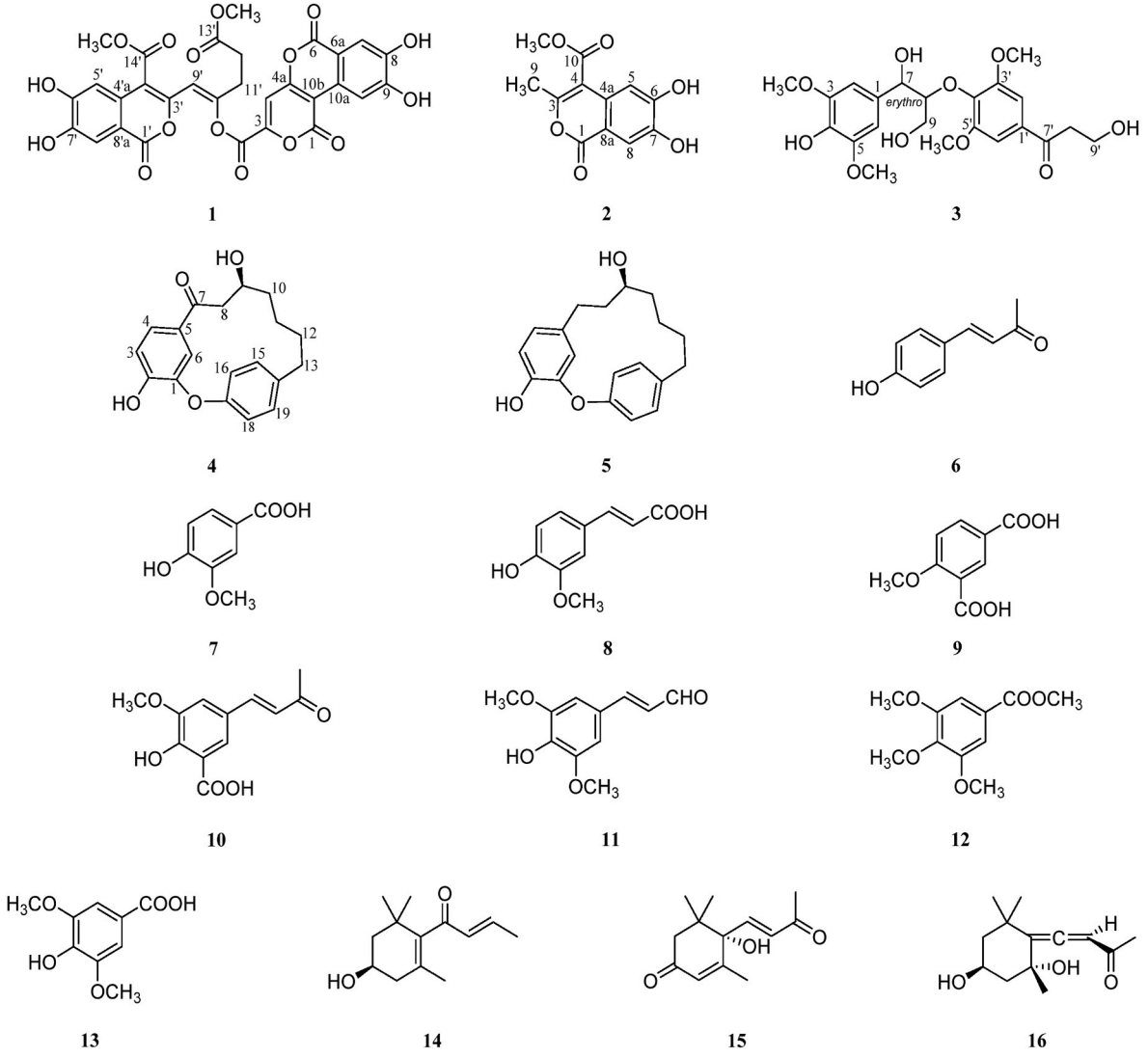

Fig. 1. Structures of compounds **1**–**16**.

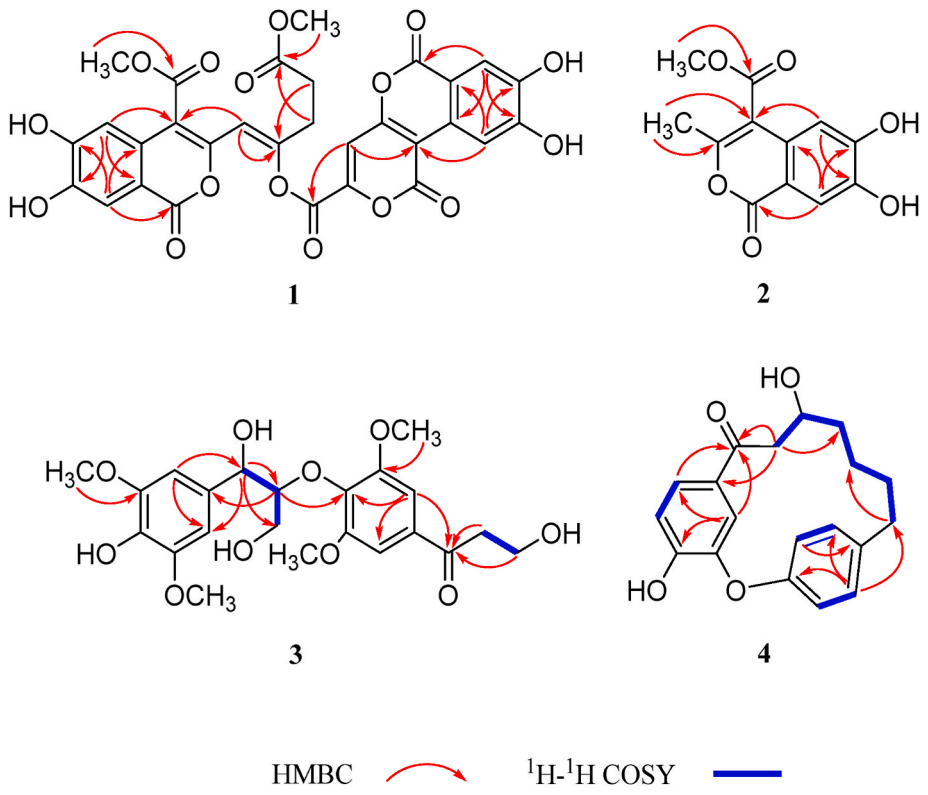

Fig. 2. Key HMBC and ^{1}H-^{1}H COSY correlations of compounds **1**–**4**.

2.8. Observation of nuclear morphology

Nuclear morphology was observed and analyzed using Hoechst 33258 (2'-(4-hydroxyphenyl)-5-(4-methyl-1-piperazinyl)-2,5′-bi-1H-benzimidazole) (Sigma) stain according to the method previously reported in the literature (Zhang et al., 2018). SH-SY5Y cells at logarithmic phase were made into cell suspension, it was inoculated into 6-well plates (Nest Biotech) at an inoculation density of 1×10^5 cells per well and incubated for 4 h. After 4 h of incubation, the upper layer of the culture medium was discarded, the cells were washed three times with phosphate buffer and subsequently stained with Hoechst 33258 (10 μg/mL). The plates were allowed to stand in the dark for 25 min at room temperature. After the staining was completed, the culture plates were placed under a fluorescent microscope to observe the nuclear morphology of the cells and photographed the results.

2.9. Mitochondrial membrane potential assay

The mitochondrial membrane potential (MMP) assay was performed like the method described in the previous report (Xu et al., 2019). Cells of exponential phase were inoculated uniformly in 6-well plates at a cell density of 1×10^5 cells per well, and 50 μmol/L of the sample was added to the dosing group, the control group and the model group were pretreated with an equal volume of blank medium for 1 h. The model group and the dosing group were incubated with 400 μmol/L H_2O_2 in 5% CO_2 at 37 °C for 4 h to injure the cells. The treated cells were washed three times using PBS and mixed with cationic fluorescent JC-1 (5,5′,6,6′-tetrachloro-1,1,3,3′-tetraethylbenzimidizolyl carbocyanine iodide) (1X) (Sigma). Furthermore, observe the changes of red and green fluorescent aggregates under a fluorescent microscope.

2.10. ECD spectral calculation

The absolute configuration of compound **4** was determined using the method of ECD calculation. Conformational analyses were performed by CONFLEX software (Conflex Corp., Carlsbad, CA, USA) in the MMFF94 force field (Li, Hou, et al., 2020). Density functional theory (DFT) calculations have been performed with the Gaussian 09w (Gaussian Inc., Wallingford, CT, USA) program package using the B3LYP/6-31G(d) level to obtain the geometry optimizations and frequency calculations (Tang et al., 2019). Subsequently, the ECD calculations of all the selected conformers were calculated using the time-dependent density functional theory (TDDFT) method at the B3LYP/6-31G(d,p) level with the polarizable continuum model (PCM) in a MeOH solution. The calculated ECD spectra were generated using SpecDis 1.51 (University of Wurzburg, Wurzburg, Germany) according to the Boltzmann weighting of each conformer (Bruhn et al., 2013).

2.11. Molecular orbital analysis

A conformational search was performed utilizing the MMFF94 force field with an energy window of 10 kJ/mol by the Spartan 20 program (Wavefunction Inc., Beijing, China). The conformations under a certain energy window were processed in the use of GaussView 5.0 software (Gaussian) and convert their formats of the files to facilitate subsequent calculations. The calculations were carried out and the highest occupied molecular orbital (HOMO) and the lowest unoccupied molecular orbital (LUMO) were analyzed in the Gaussian 09w package. Eventually, the presentations of tracks were optimized and drawn in combination with Multiwfn 3.7 (Beijing Kein Research Center for Natural Sciences, Beijing, China) and VMD 1.9.3 software (University of Illinois, Urbana, IL, USA) (Lu & Chen, 2012; Decherchi, Spitaleri, Stone, & Rocchia, 2019).

2.12. Statistical analysis

All results and data were confirmed in at least three parallel experiments. Analysis of variance (ANOVA) test using GraphPad Prism 6.0 software (GraphPad Software, San Diego, CA, USA) were used for statistical analysis and $p < 0.05$ was considered to indicate a statistical significance. The data are expressed as means ± standard deviation

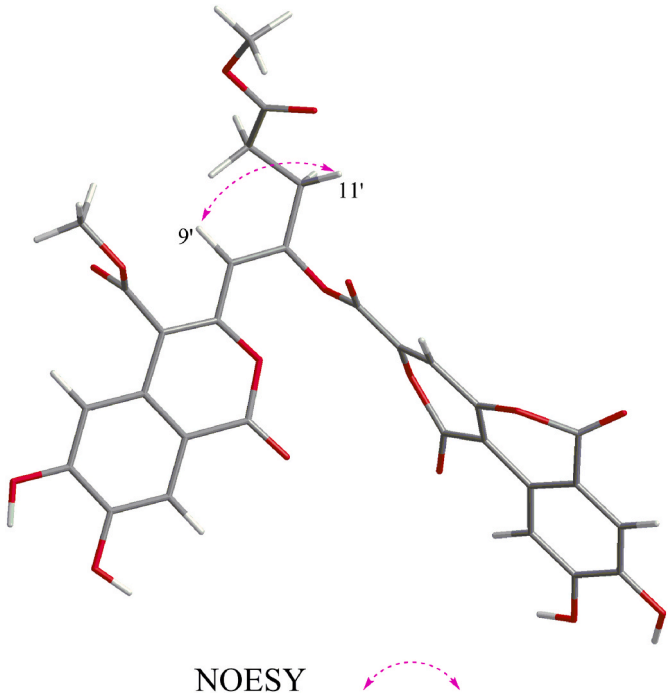

Fig. 3. NOESY correlation of **1**.

(SD).

3. Results and discussion

3.1. Elucidation of compound structures

The 70% EtOH-based extract of *I.obliquus* was subjected to a chemical investigation that consecutively provided two new isocoumarins (**1**–**2**), a new 8-*O*-4′-neolignan (**3**), a new cyclic diarylheptanoid (**4**) together with 12 known compounds (**5**–**16**) by successive flash chromatography and semipreparative HPLC. The chemical structures of these compounds are exhibited in Fig. 1.

Compound **1** was obtained as a light yellow powder with the molecular formula $C_{30}H_{20}O_{16}$, which was established from a molecular ion peak at *m/z* 659.0646 ($[M + Na]^+$, calcd 659.0644) in the HRESIMS spectrum with 21 indices of hydrogen deficiency. Five uncoupled protons δ_H 8.35 (1H, s, H-10), 8.28 (1H, s, H-5′), 7.54 (1H, s, H-7) 7.49 (1H, s, H-8′), 6.59 (1H, s, H-9′) in the low field and two methoxy protons δ_H 3.90 (3H, s), 3.62 (3H, s) were identified in the ^{1}H NMR spectrum. Besides, the ^{1}H NMR spectrum of **1** exhibited the presence of two aliphatic protons at δ_H 2.86 (2H, t, $J = 7.3$ Hz, H-11′) and 2.73 (2H, t, $J = 7.3$ Hz, H-12′), indicating that this snippet of **1** is an ethidene group. The ^{13}C NMR and heteronuclear single quantum correlation (HSQC) spectra of **1** suggested the presence of thirty carbon resonances, consisting of twenty-six sp^2 atoms and four sp^3 atoms. Two tetrasubstituted aromatic rings signals (δ_C 153.7, 153.7, 148.3, 147.0, 126.6, 125.6, 114.6, 114.4, 112.5, 111.4, 111.1, 110.5) were inferred and downfield shifts of C-9, C-6′, C-8, C-7′ (δ_C 153.7, 153.7, 148.3, 147.0) gave expressions to the *o*-oxygenated substituted fragments in two benzene rings with the aid of ^{1}H NMR spectral data. Moreover, the ^{13}C NMR of **1** showed six sp^2 carbonyl carbons (δ_C 171.9, 159.0, 158.6, 158.5, 158.4, 158.2), four sp^2 oxygen-bearing double bonds (δ_C 163.8, 160.6, 160.0, 146.5), four sp^2 double bonds (δ_C 106.3, 104.4, 99.0, 98.5), two sp^3 methylene (δ_C 30.0, 28.2), and two methoxy groups (δ_C 53.3, 51.7).

The heteronuclear multiple bond correlation (HMBC) correlations of H-8′ (δ_H 7.49) with C-1′ (δ_C 158.6), C-6′ (δ_C 153.7), C-4′a (δ_C 126.6), of H-5′ (δ_H 8.28) with C-4′ (δ_C 98.5), C-7′ (δ_C 147.0), C-8′a (δ_C 111.4), in conjunction with correlations from 14′-OCH$_3$ (δ_H 3.90) to C-14′ (δ_C 159.0) constructed the isocoumarin moiety and C-14′ placed a methyl structural fragment at C-4′ (Fig. 2). Also, the HMBC spectrum relationship between H-9′ (δ_H 6.59) and C-4′ (δ_C 98.5), C-10′ (δ_C 163.8) along with the nuclear overhauser effect spectroscopy (NOESY) correlation (Fig. 3) of H-9′ and H-11′ suggested that the location of oxygenated *cis* double-bond was determined to be at C-3′. The assignment of the methyl propionate group at C-10′ was supported by the HMBC correlations of H$_2$-11′ (δ_H 2.86) with C-13′ (δ_C 171.9), H$_2$-12′ (δ_H 2.73) with C-10′ (δ_C 163.8), C-11′ (δ_C 28.2), 13′-OCH$_3$ (δ_H 3.62) with the low-field shift of C-13′. There was another isocoumarin fragment at the other end of the compound **1**, evidenced by the HMBC correlations of H-7 (δ_H 7.54) with C-6 (δ_C 158.4), C-9 (δ_C 153.7), C-10a (δ_C 125.6), and of H-10 (δ_H 8.35) with C-8 (δ_C 148.3), C-6a (δ_C 112.5), C-10b (δ_C 104.4). Apart from the aforementioned moieties, the remaining four indices of hydrogen deficiency could be classified as a ring unit and a carbonyl group. By comparing its NMR data with phelligridin J in literature (Wang et al., 2007), it was indicated that **1** contained a 8,9-dihydroxypyrano[4,3-*c*] isochromen-4-on-3-yl fragment. Additionally, the HMBC spectrum showed an olefinic singlet at δ_H 7.37 correlated with the carbonyl carbon signal at δ_C 158.5, the oxygenated olefinic carbon signal at δ_C 146.5, and the olefinic carbon signal at δ_C 104.4, the above information indicated that the carbonyl group was attached to the pyran ring through the C-3. Therefore, the gross structure of **1** was deduced and elucidated as Phellxinye A.

Compound **2** was isolated as a brown powder, for which the molecular formula was established as $C_{12}H_{10}O_6$ by HRESIMS (positive mode) $m/z = 251.0561$ $[M + H]^+$ (calcd for $C_{12}H_{11}O_6$, 251.0550), with eight degrees of unsaturation. Analysis of ^{1}H NMR data for **2** revealed two aromatic protons at δ_H 7.04 (1H, s) and 7.43 (1H, s), indicating that **2** contained a 1,2,4,5-tetrasubstituted benzene. The ^{1}H NMR spectrum of **2** exhibited signals for a methoxyl at δ_H 3.88 (3H, s), and a methyl of the double bond at δ_H 2.31 (3H, s).

Interpretation of the ^{13}C NMR and HSQC data revealed 12 carbon signals attributable to six aromatic ring signals (δ_C 153.8, 146.9, 128.2, 113.3, 110.5, and 109.2) and six aliphatic signals (δ_C 166.1, 159.7, 155.0, 109.0, 52.4, and 18.7). The structural framework of **2** was determined by the HMBC experiment (Fig. 2), in which ^{13}C-^{1}H long-range correlations were found between H-8 and C-4a/C-6/C-1, between H-5 and C-7/C-8a, between H-9 and C-4/C-10. The position of the methyl formate group at C-4 was confirmed by the HMBC correlation from OCH$_3$-10 to C-10. Meanwhile, the assignments of the two hydroxyl groups were established based on ^{13}C NMR chemical shifts of C-6 (δ_C 153.8) and C-7 (δ_C 146.9). From the above, the planar structure of Inonotphenol A (**2**) was constructed.

Compound **3** was obtained as a yellow oil, and its molecular formula of $C_{22}H_{28}O_{10}$, with eight degrees of unsaturation, was determined by HRESIMS measurements ($[M + Na]^+$ *m/z* 475.1576, calcd for $C_{22}H_{28}O_{10}Na$, 475.1575).

The ^{1}H NMR data exhibited signals for four isolated aromatic hydrogens at δ_H 7.22 (2H, s, H-2′, and H-6′) and 6.60 (2H, s, H-2, and H-6) indicating the presence of two 1,3,4,5-tetrasubstituted aromatic rings and two oxygenated methines at δ_H 4.80 (1H, d, $J = 4.9$ Hz, H-7), 4.36 (1H, dt, $J = 4.9$, 3.5 Hz, H-8), one oxygenated methylene at δ_H 3.71 (1H, m, H-9a) and 3.49 (1H, dd, $J = 11.9$, 3.5 Hz, H-9b) attributable to a 1,2,3-propanetriol unit. The spectrum also implied the presence of two sets of couple methylenes hydrogens at δ_H 3.77 (2H, t, $J = 6.3$ Hz, H-9′), δ_H 3.13 (2H, t, $J = 6.3$ Hz, H-8′) and four methoxyl groups at δ_H 3.83 (6H, s) and 3.72 (6H, s). Meanwhile, the assignments of the 1,2,3-propanetriol unit and the ethylidene unit were also supported by the ^{1}H-^{1}H two-dimensional shift correlated spectroscopy (COSY) (Fig. 2) correlations of H-7/H-8/H-9 and H-8′/H-9′.

The 22 carbon resonances were composed of twelve aromatic carbons (δ_C 152.4, 152.4, 147.4, 147.4, 140.6, 134.4, 132.4, 131.6, 105.7, 105.7, 104.3, 104.3), a conjugated carbonyl (δ_C 197.9), three sp^3 methylenes (δ_C 60.2, 57.1, 41.2), two oxidated methines (δ_C 86.5, 72.4) and four methoxy groups (δ_C 55.9, 55.9, 56.1, 56.1). Considering the

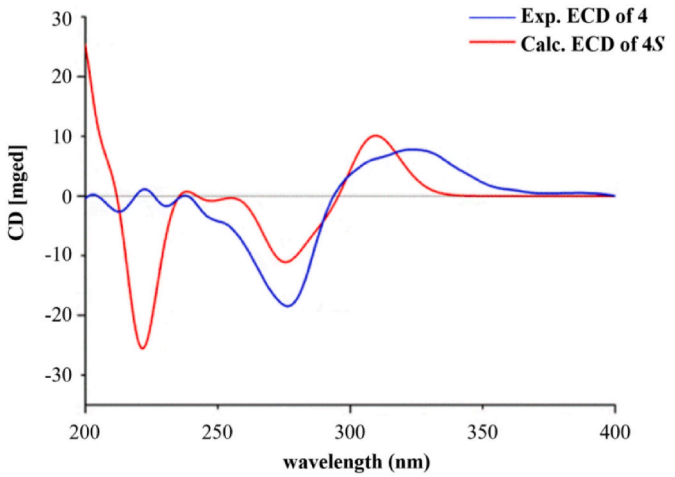

Fig. 4. Experimental and calculated ECD spectra of compound **4**.

aforementioned ^{1}H and ^{13}C NMR, it was strongly proposed that **3** might be an 8-*O*-4′-neolignan possessing two phenylpropanoid units. This assumption was also supported by the HMBC correlations of H-7 with C-2, C-6, C-8, C-9, of H-2′, H-6′, H-8′ and H-9′ with C-7′, of H-8 with C-4′. Additionally, the locations of four methoxy groups at C-3, C-5, C-3′, C-5′ were supported by the HMBC correlations of δ_H 3.72 (s, 3/5-OCH_3) with δ_C 147.4 (C-3/5), of δ_H 3.83 (s, 3′/5′-OCH_3) with δ_C 152.4 (C-3′/5′). Since the optical value of compound **3** was almost zero, it was presumed to exist in the form of a racemate.

The relative configuration of **3** was assigned as *erythro*-form, based on the small coupling constant ($J_{7,8} = 3.3$ Hz) in the ^{1}H NMR data of **3** in $CDCl_3$ (Yang et al., 2019). Therefore, the structure of *erythro*-4,7,9,9′-tetrahydroxy-3,5,3′,5′-tetramethoxy-8-*O*-4′-neolignan (**3**) was defined as shown (Fig. 1).

Compound **4** was isolated as a yellow oil. Its positive HRESIMS analysis gave an $[M + Na]^+$ ion peak at *m/z* 335.1254 (calculated for $C_{19}H_{20}O_4Na$, 335.1254), consistent with the molecular formula $C_{19}H_{20}O_4$, accounting for ten indices of hydrogen deficiency. The UV spectrum showed absorption bands at 277 nm suggesting that **4** was a biphenyl ether-type cyclic diarylheptanoid compound (Nagumo et al., 1993).

The ^{1}H NMR data displayed diagnostic signals for one 1,2,4-trisubstituted benzene ring at δ_H 7.52 (1H, dd, $J = 8.4$, 2.1 Hz, H-4), δ_H 7.02 (1H, d, $J = 8.4$ Hz, H-3), δ_H 6.03 (1H, d, $J = 2.1$ Hz, H-6), and one *para*-disubstituted benzene ring at δ_H 7.31 (1H, overlap, H-15), δ_H 7.31 (1H, overlap, H-19), δ_H 7.20 (1H, dd, $J = 8.5$, 2.5 Hz, H-16), δ_H 6.96 (1H, dd, $J = 8.7$, 2.5 Hz, H-18). With the assistance of ^{1}H-^{1}H COSY correlations of H_2-13/H_2-12/H_2-11/H_2-10/H-9/H_2-8, five methylenes, and an oxygen-bearing methine group were identified in the ^{1}H NMR spectrum.

The ^{13}C and HSQC NMR spectra revealed the presence of twelve aromatic carbons (δ_C 154.3, 149.6, 148.6, 141.4, 132.0, 131.3, 129.5, 123.7, 123.2, 122.8, 117.4, 116.3), one carbonyl group (δ_C 199.1), five sp^3 secondary carbons (δ_C 46.6, 37.5, 35.0, 32.3, 21.8) and an oxygenated sp^3 tertiary carbon (δ_C 70.1), respectively. The substitution of one carbonyl position was verified by H-4/C-7, H-6/C-7, and H-8/C-7 key HMBC correlations (Fig. 2). The hydroxyl group was then located at C-9 supported by the key H_2-10/H-9/H_2-8 COSY correlations. Therefore, the 2D structure of **4** was defined as depicted.

The absolute configuration of **4** was assigned according to a comparison of experimental and theoretical ECD spectra utilizing the TDDFT method. The computed ECD curve of (9*S*)-**4** was well-matched with the experimental data (Fig. 4). Hence, the absolute configuration of **4** was elucidated as 9*S* and named (9*S*)-acerogenin M.

Additionally, 12 known compounds were isolated and characterized by comparing with the reported 1D NMR data in the literature. Compounds **5**–**16** were respectively identified as (−)-(*S*)-acerogenin B (**5**) (Morikawa et al., 2003), 4-hydroxybenzalacetone (**6**) (Kwon et al., 2016), vanillic acid (**7**) (Li et al., 2012), (*E*)-4-Hydroxy-3-methoxycinnamic acid (**8**) (Zhao et al., 2017), 4-Methoxyisophthalic acid (**9**) (Liu et al., 2017), 2-Hydroxy-3-methoxy-5-(3-oxo-1-buten-1-yl)benzoic acid (**10**) (Profft & Sacharow, 1965), sinapaldehyde (**11**) (Lakornwong et al., 2018), tri-*O*-methylgallate (**12**) (Ito et al., 2014), syringic acid (**13**) (Huang et al., 2019), (3*S*,8*E*)-3-hydroxy-*β*-damascone (**14**) (Baumes et al., 1994), 6-hydroxy-4,7-megastigmadiene-3,9-dione (**15**) (Metuno et al., 2008), grasshopper ketone (**16**) (Uyen et al., 2020).

Table 1
Antioxidant activities of compounds **1**–**16** from Chaga mushroom *I. obliquus*.

compound	DPPH[b,c]	ABTS[b,c]	FRAP[b,d]
1	33.45 ± 1.22	55.03 ± 0.94	588.33 ± 23.97
2	49.35 ± 2.55	64.24 ± 1.25	402.88 ± 28.32
3	86.96 ± 0.64	152.11 ± 1.29	228.40 ± 10.45
4	45.46 ± 1.43	40.51 ± 0.54	215.21 ± 18.46
5	55.45 ± 0.73	84.66 ± 1.75	376.43 ± 13.49
6	116.90 ± 1.22	178.13 ± 2.35	569.76 ± 30.24
7	NA	148.49 ± 1.31	105.79 ± 9.56
8	52.55 ± 0.83	50.33 ± 1.24	432.48 ± 25.14
9	106.90 ± 0.82	84.25 ± 1.24	104.36 ± 12.46
10	NA	NA	122.64 ± 10.38
11	170.78 ± 2.01	NA	556.64 ± 29.67
12	NA	190.33 ± 3.04	317.03 ± 14.55
13	44.26 ± 0.99	NA	467.05 ± 19.03
14	50.78 ± 0.88	90.58 ± 1.04	308.11 ± 16.50
15	48.98 ± 2.36	103.72 ± 2.07	224.74 ± 23.08
16	67.27 ± 1.51	135.77 ± 2.24	329.62 ± 25.69
Trolox	23.04 ± 1.14	72.99 ± 1.02	737.23 ± 33.65

aNA: Not active.
[b] Results represent means ± SD (n = 3) and all values are significantly different ($p < 0.05$).
[c] DPPH and ABTS: concentration in μmol/L required to scavenge 50% of the free radical.
[d] FRAP: concentration in μmol Trolox/g DW.

3.2. Antioxidant activities in vitro

Free radicals are products of metabolic pathways and contain molecules with one or more unpaired electrons. Under physiological conditions, there is a balance between the production and scavenging of free radicals in the body. Antioxidants, also known as free radical scavengers, can eliminate OS and some of them have been used as neuroprotectants to prevent disease of the central nervous system (Pearson-Smith & Patel, 2020). The mushroom *I.obliquus* had antioxidant capacity according to the previous literature (Eid & Das, 2020; Xu et al., 2011), and the antioxidative effects of natural foods were beneficial to human health to a certain extent. Therefore, the isolated 16 monomer compounds were proposed to discover their activities against free radicals *in vitro*. The free radical scavenging effects were directly analyzed with DPPH, ABTS, and FRAP methods, as summarized in Table 1.

In the DPPH assay, with Trolox ($IC_{50} = 23.04 \pm 1.14$ μmol/L) as the positive control, tested compound **1** ($IC_{50} = 33.45 \pm 1.22$ μmol/L) exhibited preferable antioxidant activity, and compounds **13**, **4**, **15** and **2** presented moderate activities with IC_{50} values of 44.26 ± 0.99, 45.46 ± 1.43, 48.98 ± 2.36 and 49.35 ± 2.55 μmol/L, respectively. According to the results of ABTS assay, compounds **4** ($IC_{50} = 40.51 \pm 0.54$ μmol/L), **8** ($IC_{50} = 50.33 \pm 1.24$ μmol/L), **1** ($IC_{50} = 55.03 \pm 0.94$ μmol/L) and **2** ($IC_{50} = 64.24 \pm 1.25$ μmol/L) had significant free radical scavenging abilities comparable to that of the positive drug. Obviously, **4** had the remarkable capacity to scavenge free radicals, **5** ($IC_{50} = 84.66 \pm 1.75$ μmol/L) and **9** ($IC_{50} = 84.25 \pm 1.24$ μmol/L) showed potent activities being comparable with that of the positive control Trolox ($IC_{50} = 72.99 \pm 1.02$ μmol/L). FRAP evaluation results revealed that compounds **1** (588.33 ± 23.97 μmol Trolox/g DW), **6** (569.76 ± 30.24 μmol Trolox/g DW) and **11** (556.64 ± 29.67 μmol Trolox/g DW) displayed noticeable

Table 2
Coefficient of determination (R^2) among DPPH, ABTS and FRAP assays.

R^2 ($p < 0.05$)	DPPH values	ABTS values	FRAP values
DPPH values	1.000	0.687	0.894
ABTS values	0.687	1.000	0.876
FRAP values	0.894	0.876	1.000

Results represent means ± SD (n = 3) and all values are significantly different ($p < 0.05$).

effects on total reducing capacities and the reducing ability of compound **1** was particularly outstanding. Beyond that, metabolites **2** (402.88 ± 28.32 μmol Trolox/g DW), **8** (432.48 ± 25.14 μmol Trolox/g DW) and **13** (467.05 ± 19.03 μmol Trolox/g DW) exerted moderate potent radical-scavenging properties against FRAP.

Afterwards, the correlations between three experimental methods were carried out using GraphPad Prism 6.0 software. The results (Table 2) of this provided a medium-high coefficient of determination between DPPH, ABTS, and FRAP assays. This indicated that the variability of the above three methods was small and it was consistent with the previously reported study (Huang et al., 2014). Therefore, through the comprehensive analysis of the above three chemical antioxidant capacity tests, compound **1** was a prominent antioxidant component and **2** was also a medium bioactive constituent contributing to antioxidant capacity.

3.3. Neuroprotective effect in H_2O_2-induced SH-SY5Y cells

The use of antioxidants to scavenge excess free radicals is one of the strategies in the clinical treatment of neurological diseases (Neha et al., 2019). Herein, two selected compounds with preferable antioxidant activities were tested for neuroprotection. Compounds **1** and **2** were tested for their neuroprotective effects against the H_2O_2-induced SH-SY5Y cell line, using an MTT assay, with Trolox as the positive control. Only compound **1** exhibited a significant neuroprotective effect *in vitro* with survival rates of 96.75% at 50 μmol/L and 66.00% at 25 μmol/L as compared to the positive control.

3.4. Neuroprotective effect against H_2O_2-induced SH-SY5Y cells apoptosis

The definition of apoptotic cells is based on changes in nuclear morphology, such as chromatin condensation and breakage of chromatin (Kijima et al., 2019). Hoechst 33258 had the ability to show apoptosis, and the apoptosis was detected by the fluorescence degree and morphology of the cell nucleus (Zhou et al., 2018). To further, comprehend the mechanism for protecting H_2O_2-induced SH-SY5Y cells, the apoptotic morphology was operated. The phenomenon showed that the blue fluorescence of compound **1** at concentrations of 12.5, 25 and 50 μmol/L was significantly weakened after staining the cell nucleus with Hoechst 33258 (Fig. 5A). Besides, the decreased expressions of nuclear shrinkage, chromatin condensation, and fragmentation were induced by H_2O_2. This result from the above morphological observations indicated that compound **1** exerted a neuroprotective effect against H_2O_2-induced SH-SY5Y cells by reducing apoptosis.

3.5. Neuroprotective effect of compound 1 against the mitochondrial damage

The decrease of MMP is commonly used as an important indicator of early cell apoptosis. To assess the role of compound **1** in mitochondrial dysfunction, JC-1 staining was used to detect the changes of MMP (Wang et al., 2020). Tested **1** treated in 12.5, 25 and 50 μmol/L, as demonstrated by their prominent red fluorescence in a dose-dependent manner, whereas cells treated with H_2O_2 in the model group exhibited green fluorescence (Fig. 5B). Therefore, based on the aforementioned results under a fluorescence microscope confirmed that the protective effect of **1** against H_2O_2-induced apoptosis.

3.6. Identification of bonding sites by molecular orbital analysis

ROS may lead to lipid peroxidation, which injures neurotransmitter signaling and further worsens the functions of the nervous system (Bhat et al., 2015). To a certain extent, secondary metabolites with strong free radical scavenging abilities have relatively protective effects of SH-SY5Y cells caused by H_2O_2-induced OS (Wang et al., 2019). The objective of the molecular orbital analysis was further to expound on the functional groups that can produce chemical reactions (Veiko et al., 2021). The computational studies were performed by operating the Gaussian 09

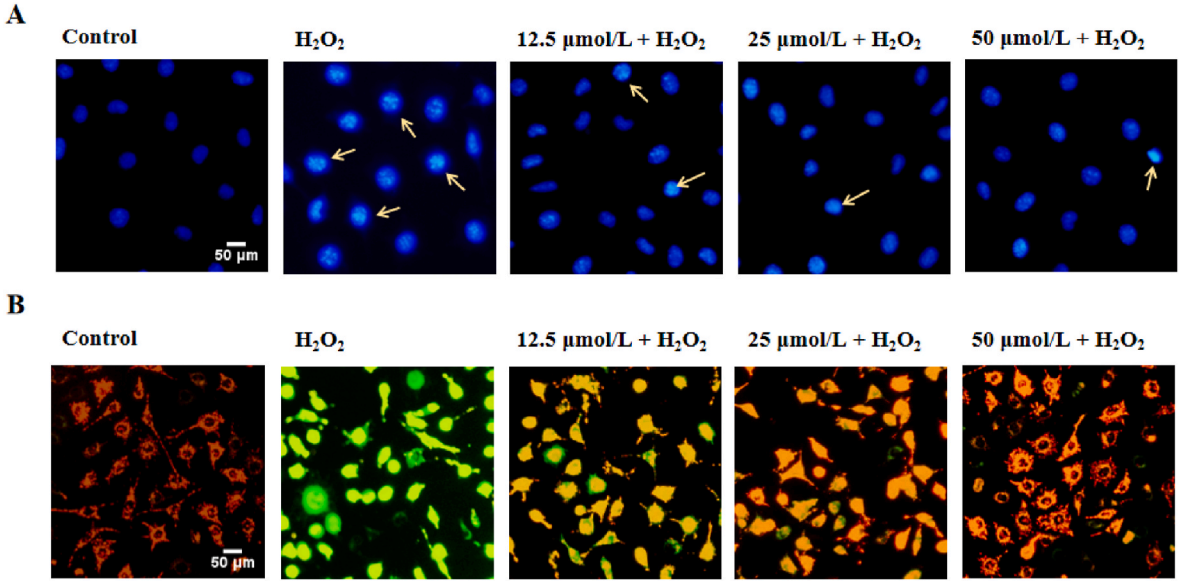

Fig. 5. (A) Observation of compound **1** (12.5, 25 and 50 μmol/L) on morphological changes of H_2O_2-treated SH-SY5Y cells. **(B)** Compound **1** (12.5, 25 and 50 μmol/L) reduced mitochondrial dysfunction in H_2O_2-treated SH-SY5Y cells.

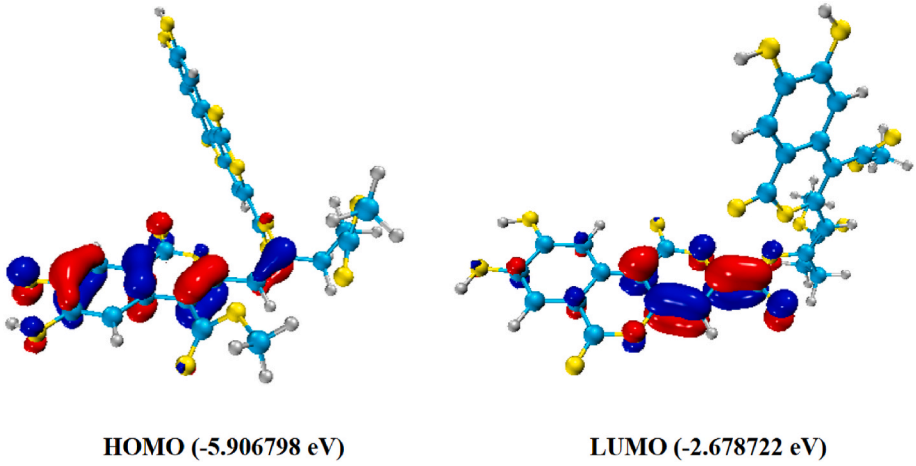

Fig. 6. The HOMO and LUMO distributions for compound **1**.

software package. Full geometry optimizations were carried out using DFT at the B3LYP level for compound **1**. The parts of the molecule that tend to donate or lose electrons are indicated by HOMO and LUMO. In general, HOMO is an extremely significant marker to investigate the free radical scavenging potential (Yang et al., 2021). The HOMO molecular orbital of **1** may indicate its active sites of the free radical elimination due to an isocoumarin fragment and an oxygenated *cis* double-bond after electron transfer (Fig. 6) and the value of energy difference of the frontier molecular orbitals (HOMO − LUMO) about 3.228076 eV. This process was calculated at the Multiwfn software (Lu & Chen, 2012) and beautified with VMD software.

4. Conclusion

The chemical investigations of the Chaga mushroom *I. obliquus* led to the isolation of four new compounds (**1**–**4**) along with 12 known compounds (**5**–**16**) from the EtOAc-fraction. Compounds **1** and **2** had antioxidant activities compared to Trolox, and **1** was effective in ameliorating H_2O_2-induced nerve damage by increasing cells viability and preventing mitochondrial damage in SH-SY5Y cells. Furthermore, the isocoumarin fragment and an oxygenated *cis* double-bond might be the active sites of secondary metabolite **1** to eliminate the OS and exert neuroprotective activity. In this sense, **1** as a potential natural source of neuroprotective and antioxidant compound that possesses health benefits against nerve damage and OS, is able to be used as raw material for nutritional, dietary antioxidant supplements and neuroprotectants.

Author contributions

Y. Chang, M. Bai, X. X. Huang, and S. J. Song designed the steps of the experiment. Y. Chang, M. Bai, and C. X. Zou performed the chemical experiments and analyzed the data. Y. Chang and X. B. Xue performed the pharmacology experiments. Y. Chang drafted the manuscript. M. Bai and X. X. Huang altered some issues in the manuscript. The manuscript was a combination of all authors' contributions and all authors agreed to its final version.

Declaration of competing interest

The authors declare that they have no known competing financial interests or personal relationships that could have appeared to influence the work reported in this paper.

Acknowledgements

This work was supported by China Postdoctoral Science Foundation (2020M680987), Science and Technology Planning Project of Liaoning Province (2021JH1/10400049), Career Development Support Plan for Young and Middle-aged Teachers in Shenyang Pharmaceutical University (ZQN2018006), and the Project of Innovation Team Foundation (LT2015027).

Appendix A. Supplementary data

Supplementary data to this article can be found online at https://doi.org/10.1016/j.fbio.2022.101623.

References

Albarracin, S. L., Stab, B., Casas, Z., Sutachan, J. J., Samudio, I., Gonzalez, J., Gonzalo, L., Capani, F., Morales, L., & Barreto, G. E. (2012). Effects of natural antioxidants in neurodegenerative disease. *Nutritional Neuroscience, 15*, 1–9. https://doi.org/10.1179/1476830511Y.0000000028

Alkadi, H. (2020). A review on free radicals and antioxidants. *Infectious Disorders Drug Targets, 20*, 16–26. https://doi.org/10.2174/1871526518666180628124323

Baumes, R. L., Aubert, C. C., Günata, Z. Y., Moor, W. D., Bayonove, C. L., & Tapiero, C. (1994). Structures of two C_{13}-norisoprenoid glucosidic precursors of wine flavor. *Journal of Essential Oil Research, 6*, 587–599. https://doi.org/10.1080/10412905.1994.9699350

Bhat, A. H., Dar, K. B., Anees, S., Zargar, M. A., Masood, A., Sofi, M. A., & Ganie, S. A. (2015). Oxidative stress, mitochondrial dysfunction and neurodegenerative diseases; a mechanistic insight. *Biomedicine & Pharmacotherapy, 74*, 101–110. https://doi.org/10.1016/j.biopha.2015.07.025

Bruhn, T., Schaumlöffel, A., Hemberger, Y., & Bringmann, G. (2013). SpecDis: Quantifying the comparison of calculated and experimental electronic circular dichroism spectra. *Chirality, 25*, 243–249. https://doi.org/10.1002/chir.22138

Chen, H., Liou, B. K., Hsu, K. C., Chen, C. S., & Chuang, P. T. (2021). Implementation of food safety management systems that meets ISO 22000:2018 and HACCP: A case study of capsule biotechnology products of chaga mushroom. *Journal of Food Science, 86*, 40–54. https://doi.org/10.1111/1750-3841.15553

Decherchi, S., Spitaleri, A., Stone, J., & Rocchia, W. (2019). NanoShaper-VMD interface: Computing and visualizing surfaces, pockets and channels in molecular systems. *Bioinformatics (Oxford, England), 35*, 1241–1243. https://doi.org/10.1093/bioinformatics/bty761

Di Meo, S., & Venditti, P. (2020). Evolution of the knowledge of free radicals and other oxidants, 2020 *Oxidative Medicine and Cellular Longevity*. , Article 9829176. https://doi.org/10.1155/2020/9829176.

Eid, J. I., & Das, B. (2020). Molecular insights and cell cycle assessment upon exposure to Chaga (*Inonotus obliquus*) mushroom polysaccharides in zebrafish (*Danio rerio*). *Scientific Reports, 10*, 7406. https://doi.org/10.1038/s41598-020-64157-3

Ghalkhani, A., Moradkhani, S., Soleimani, M., & Dastan, D. (2021). Functional components, antibacterial, antioxidant, and cytotoxic activities of *Lamium garganicum* L. ssp. *pictum* as a novel natural agents from lamiaceae family. *Food Bioscience, 43*, Article 101265. https://doi.org/10.1016/j.fbio.2021.101265

Huang, H. C., Chen, L. C., Chang, T. H., Zhu, T. F., Chen, C. L., Cheng, M. J., & Chen, J. J. (2019). A new lignanamide derivative and bioactive constituents of *Lycium chinense*. *Chemistry of Natural Compounds, 55*, 1002–1006. https://doi.org/10.1007/s10600-019-02879-1

Huang, H. Z., Sun, Y. J., Lou, S. T., Li, H., & Ye, X. Q. (2014). *In vitro* digestion combined with cellular assay to determine the antioxidant activity in Chinese bayberry (*Myrica rubra* Sieb. Et Zucc.) fruits: A comparison with traditional methods. *Food Chemistry, 146*, 363–370. https://doi.org/10.1016/j.foodchem.2013.09.071

Ito, H., Li, P., Koreishi, M., Nagatomo, A., Nishida, N., & Yoshida, T. (2014). Ellagitannin oligomers and a neolignan from pomegranate arils and their inhibitory effects on the formation of advanced glycation end products. *Food Chemistry, 152*, 323–330. https://doi.org/10.1016/j.foodchem.2013.11.160

Kijima, M., Yamagishi, H., Hara, Y., Kasai, M., Takami, Y., Takemura, H., Miyanari, Y., Shinkai, Y., & Mizuta, R. (2019). Histone H1 quantity determines the efficiency of chromatin condensation in both apoptotic and live cells. *Biochemical and Biophysical Research Communications, 512*, 202–207. https://doi.org/10.1016/j.bbrc.2019.03.030

Kwon, J., Hiep, N. T., Kim, D. W., Hong, S., Guo, Y., Hwang, B. Y., Lee, H. J., Mar, W., & Lee, D. (2016). Chemical constituents isolated from the root bark of *Cudrania tricuspidata* and their potential neuroprotective effects. *Journal of Natural Products, 79*, 1938–1951. https://doi.org/10.1021/acs.jnatprod.6b00204

Lakornwong, W., Kanokmedhakul, K., & Kanokmedhakul, S. (2018). A new coruleoellagic acid derivative from stems of *Rhodamnia dumetorum*. *Natural Product Research, 32*, 1653–1659. https://doi.org/10.1080/14786419.2017.1395430

Lee, I. K., Kim, Y. S., Jang, Y. W., Jung, J. Y., & Yun, B. S. (2007). New antioxidant polyphenols from the medicinal mushroom *Inonotus obliquus*. *Bioorganic & Medicinal Chemistry Letters, 17*, 6678–6681. https://doi.org/10.1016/j.bmcl.2007.10.072

Liang, L. Y., Zhang, Z. S., & Wang, H. (2009). Antioxidant activities of extracts and subfractions from *Inonotus Obliquus*. *International Journal of Food Sciences and Nutrition, 60*, 175–184. https://doi.org/10.1080/09637480903042279

Li, X., Cao, W., Shen, Y., Li, N., Dong, X. P., Wang, K. J., & Cheng, Y. X. (2012). Antioxidant compounds from *Rosa laevigata* fruits. *Food Chemistry, 130*, 575–580. https://doi.org/10.1016/j.foodchem.2011.07.076

Li, S. S., Hou, Z. L., Yao, G. D., Guo, R., Wang, Y. X., Lin, B., Huang, X. X., & Song, S. J. (2020). Lignans and neolignans with isovaleroyloxy moiety from *Solanum lyratum* Thunb.: Chiral resolution, configurational assignment and neuroprotective effects. *Phytochemistry, 178*, Article 112461. https://doi.org/10.1016/j.phytochem.2020.112461

Li, N. N., Jiang, H. C., Yang, J., Wang, C. Y., Wu, L. Y., & Hao, Y. X. (2021). Characterization of phenolic compounds and anti-acetylcholinase activity of coconut shells. *Food Bioscience, 42*, Article 101204. https://doi.org/10.1016/j.fbio.2021.101204

Li, W., Lu, Q. L., Li, X., Liu, H. C., Sun, L. D., Lu, X., Zhao, Y. Q., & Liu, P. (2020). Anti-alzheimer's disease activity of secondary metabolites from *Xanthoceras sorbifolia* Bunge. *Food & Function, 11*, 2067–2079. https://doi.org/10.1039/c9fo01138b

Liu, Y., Liu, H. Y., Xia, Y., Guo, H., He, X. Q., Li, H., Wu, D. T., Geng, F., Lin, F. J., Li, H. B., Zhuang, Q. G., & Gan, R. Y. (2021). Screening and process optimization of ultrasound-assisted extraction of main antioxidants from sweet tea (*Lithocarpus litseifolius* [Hance] Chun). *Food Bioscience, 43*, Article 101277. https://doi.org/10.1016/j.fbio.2021.101277

Liu, X. J., Yan, Y. N., Wang, S. Q., Li, X., & Liu, X. G. (2017). New synthesis of 4-methoxyisophthalic acid. *Russian Journal of Organic Chemistry, 53*, 459–461. https://doi.org/10.1134/S1070428017030241

Lu, T., & Chen, F. (2012). Multiwfn: A multifunctional wavefunction analyzer. *Journal of Computational Chemistry, 33*, 580–592. https://doi.org/10.1002/jcc.22885

Ma, L. S., Chen, H. X., Dong, P., & Lu, X. M. (2013). Anti-inflammatory and anticancer activities of extracts and compounds from the mushroom *Inonotus obliquus*. *Food Chemistry, 139*, 503–508. https://doi.org/10.1016/j.foodchem.2013.01.030

Metuno, R., Ngandeu, F., Tchinda, A. T., Ngameni, B., Kapche, G. D. W. F., Djemgou, P. C., Ngadjui, B. T., Bezabih, M., & Abegaz, B. M. (2008). Chemical constituents of *Treculia acuminata* and *Treculia africana* (Moraceae). *Biochemical Systematics & Ecology, 36*, 148–152. https://doi.org/10.1016/j.bse.2007.06.012

Morikawa, T., Tao, J., Toguchida, I., Matsuda, H., & Yoshikawa, M. (2003). Structures of new cyclic diarylheptanoids and inhibitors of nitric oxide production from Japanese folk medicine. *Acer nikoense*. *Journal of Natural Products, 66*, 86–91. https://doi.org/10.1021/np020351m

Nagumo, S., Kaji, N., Inoue, T., & Nagai, M. (1993). Studies on the Constituents of Aceraceae plants. XI. two types of cyclic diarylheptanoid from *Acer nikoense*. *Chemical & Pharmaceutical Bulletin, 41*, 1255–1257. https://doi.org/10.1248/cpb.41.1255

Neha, K., Haider, M. R., Pathak, A., & Yar, M. S. (2019). Medicinal prospects of antioxidants: A review. *European Journal of Medicinal Chemistry, 178*, 687–704. https://doi.org/10.1016/j.ejmech.2019.06.010

Otmani, A., Amessis-Ouchemoukh, N., Birinci, C., Yahiaoui, S., Kolayli, S., Rodríguez-Flores, M. S., Escuredo, O., Seijo, M. C., & Ouchemoukh, S. (2021). Phenolic compounds and antioxidant and antibacterial activities of Algerian honeys. *Food Bioscience, 42*, Article 101070. https://doi.org/10.1016/j.fbio.2021.101070

Pearson-Smith, J. N., & Patel, M. (2020). Antioxidant drug therapy as a neuroprotective countermeasure of nerve agent toxicity. *Neurobiology of Disease, 133*, Article 104457. https://doi.org/10.1016/j.nbd.2019.04.013

Profft, E., & Sacharow, L. (1965). Zur kenntnis des o-vanillins. vi. kondensationsreaktionen des 5-carboxyvanillins. *Advanced Synthesis & Catalysis, 28*, 99–107. https://doi.org/10.1002/prac.19650280111

Radi, E., Formichi, P., Battisti, C., & Federico, A. (2014). Apoptosis and oxidative stress in neurodegenerative diseases. *Journal of Alzheimer's Disease, 42*(3), S125–S152. https://doi.org/10.3233/JAD-132738

Tang, J. W., Xu, H. C., Wang, W. G., Hu, K., Zhou, Y. F., Chen, R., Li, X. N., Du, X., Sun, H. D., & Puno, P. T. (2019). (+)- and (-)-Alternarilactone A: Enantiomers with a diepoxy-cage-like scaffold from an Endophytic *Alternaria* sp. *Journal of Natural Products, 82*, 735–740. https://doi.org/10.1021/acs.jnatprod.8b00571

Uyen, N. H., Widyowati, R., Sulistyowaty, M. I., Sugimoto, S., Yamano, Y., Kawakami, S., Otsuka, H., & Matsunami, K. (2020). Firmosides A and B: Two new sucrose ferulates from the aerial parts of *Silene firma* and evaluation of radical scavenging activities. *Journal of Natural Medicines, 74*, 796–803. https://doi.org/10.1007/s11418-020-01426-5

Veiko, A. G., Lapshina, E. A., & Zavodnik, I. B. (2021). Comparative analysis of molecular properties and reactions with oxidants for quercetin, catechin, and naringenin. *Molecular and Cellular Biochemistry, 476*, 4287–4299. https://doi.org/10.1007/s11010-021-04243-w

Wang, C., Li, W. W., Chen, Z. Q., Gao, X. D., Yuan, G. Q., Pan, Y. X., & Chen, H. X. (2018). Effects of simulated gastrointestinal digestion in vitro on the chemical properties, antioxidant activity, α-amylase and α-glucosidase inhibitory activity of polysaccharides from *Inonotus obliquus*. *Food Research International (Ottawa, Ont), 103*, 280–288. https://doi.org/10.1016/j.foodres.2017.10.058

Wang, J., Liu, Q. B., Hou, Z. L., Shi, S. C., Ren, H., Yao, G. D., Lin, B., Huang, X. X., & Song, S. J. (2020). Discovery of guaiane-type sesquiterpenoids from the roots of *Daphne genkwa* with neuroprotective effects. *Bioorganic Chemistry, 95*, Article 103545. https://doi.org/10.1016/j.bioorg.2019.103545

Wang, C. F., Liu, X. M., Lian, C. L., Ke, J. Y., & Liu, J. Q. (2019). Triterpenes and aromatic meroterpenoids with antioxidant activity and neuroprotective effects from *Ganoderma lucidum*. *Molecules (Basel, Switzerland), 24*, 4353. https://doi.org/10.3390/molecules24234353

Wang, Y., Shang, X. Y., Wang, S. J., Mo, S. Y., Li, S., Yang, Y. C., Ye, F., Shi, J. G., & He, L. (2007). Structures, biogenesis, and biological activities of pyrano[4,3-c]isochromen-4-one derivatives from the fungus *Phellinus igniarius*. *Journal of Natural Products, 70*, 296–299. https://doi.org/10.1021/np060476h

Xiang, Y. L., Xu, X. Q., & Li, J. (2012). Chemical properties and antioxidant activity of exopolysaccharides fractions from mycelial culture of *Inonotus obliquus* in a ground corn stover medium. *Food Chemistry, 134*, 1899–1905. https://doi.org/10.1016/j.foodchem.2012.03.121

Xu, F. B., Wang, P. Y., Yao, Q. C., Shao, B., Yu, H. Y., Yu, K. Y., & Li, Y. F. (2019). Lycopene alleviates AFB1-induced immunosuppression by inhibiting oxidative stress and apoptosis in the spleen of mice. *Food & Function, 10*, 3868–3879. https://doi.org/10.1039/c8fo02300j

Xu, X., Wu, Y., & Hui, C. (2011). Comparative antioxidative characteristics of polysaccharide-enriched extracts from natural sclerotia and cultured mycelia in submerged fermentation of *Inonotus obliquus*. *Food Chemistry, 127*, 74–79. https://doi.org/10.1016/j.foodchem.2010.12.090

Yang, J., Chen, J. X., Hao, Y. X., & Liu, Y. P. (2021). Identification of the DPPH radical scavenging reaction adducts of ferulic acid and sinapic acid and their structure-antioxidant activity relationship. *LWT, 146*, Article 111411. https://doi.org/10.1016/j.lwt.2021.111411

Yang, Y. N., Han, B., Yang, P. F., Feng, Z. M., Jiang, J. S., & Zhang, P. C. (2019). A concise approach for determining the relative configuration of H-7 and H-8 in 8,4'-oxyneolignans by 1H NMR spectroscopy. *Organic Chemistry Frontiers, 6*, 886–891. https://doi.org/10.1039/C8QO01155A

Yu, J., Xiang, H. Y., & Xie, Q. H. (2020). The difference of regulatory effect of two *Inonotus obliquus* extracts on high-fat diet mice in relation to the fatty acid elongation function of gut microbiota. *Food Science & Nutrition, 9*, 449–458. https://doi.org/10.1002/fsn3.2012

Zhang, Y., Wang, W., He, H., Song, X. Y., Yao, G. D., & Song, S. J. (2018). Triterpene saponins with neuroprotective effects from a wild vegetable *Aralia elata*. *Journal of Functional Foods, 45*, 313–320. https://doi.org/10.1016/j.jff.2018.04.026

Zhao, J. Q., Wang, Y. M., Yang, Y. L., Zeng, Y., Mei, L. J., Shi, Y. P., & Tao, Y. D. (2017). Antioxidants and α-glucosidase inhibitors from "Liucha" (young leaves and shoots of *Sibiraea laevigata*). *Food Chemistry, 230*, 117–124. https://doi.org/10.1016/j.foodchem.2017.03.024

Zheng, W. F., Miao, K. J., Liu, Y. B., Zhao, Y. X., Zhang, M. M., Pan, S. Y., & Dai, Y. C. (2010). Chemical diversity of biologically active metabolites in the sclerotia of *Inonotus obliquus* and submerged culture strategies for up-regulating their production. *Applied Microbiology and Biotechnology, 87*, 1237–1254. https://doi.org/10.1007/s00253-010-2682-4

Zhou, L., Yao, G. D., Song, X. Y., Wang, J., Lin, B., Wang, X. B., Huang, X. X., & Song, S. J. (2018). Neuroprotective effects of 1,2-diarylpropane type phenylpropanoid enantiomers from red raspberry against H_2O_2-induced oxidative stress in human neuroblastoma SH-SY5Y cells. *Journal of Agricultural and Food Chemistry, 66*, 331–338. https://doi.org/10.1021/acs.jafc.7b04430

Zia, M. P., & Alibas, I. (2021). Influence of the drying methods on color, vitamin C, anthocyanin, phenolic compounds, antioxidant activity, and *in vitro* bioaccessibility of blueberry fruits. *Food Bioscience, 42*, Article 101179. https://doi.org/10.1016/j.fbio.2021.101179

Zuriarrain-Ocio, A., Zuriarrain, J., Vidal, M., Dueñas, M. T., & Berregi, I. (2021). Antioxidant activity and phenolic profiles of ciders from the Basque Country. *Food Bioscience, 41*, Article 100887. https://doi.org/10.1016/j.fbio.2021.100887